Redox chemistry changes in the Panthalassic Ocean linked to the end-Permian mass extinction and delayed Early Triassic biotic recovery

Guijie Zhang[a], Xiaolin Zhang[a], Dongping Hu[a], Dandan Li[a], Thomas J. Algeo[b], James Farquhar[c], Charles M. Henderson[d], Liping Qin[a], Megan Shen[e], Danielle Shen[e], Shane D. Schoepfer[d], Kefan Chen[a], and Yanan Shen[a,1]

[a]School of Earth and Space Sciences, University of Science and Technology of China, Hefei 230026, China; [b]Department of Geology, University of Cincinnati, Cincinnati, OH 45221; [c]Department of Geology & Earth System Science Interdisciplinary Center, University of Maryland, College Park, MD 20742; [d]Department of Geoscience, University of Calgary, Calgary, AB, Canada T2N 1N4; and [e]Thomas S. Wootton High School, Rockville, MD 20850

Edited by Mark H. Thiemens, University of California at San Diego, La Jolla, CA, and approved December 23, 2016 (received for review July 5, 2016)

The end-Permian mass extinction represents the most severe biotic crisis for the last 540 million years, and the marine ecosystem recovery from this extinction was protracted, spanning the entirety of the Early Triassic and possibly longer. Numerous studies from the low-latitude Paleotethys and high-latitude Boreal oceans have examined the possible link between ocean chemistry changes and the end-Permian mass extinction. However, redox chemistry changes in the Panthalassic Ocean, comprising ∼85–90% of the global ocean area, remain under debate. Here, we report multiple S-isotopic data of pyrite from Upper Permian–Lower Triassic deep-sea sediments of the Panthalassic Ocean, now present in outcrops of western Canada and Japan. We find a sulfur isotope signal of negative $\Delta^{33}S$ with either positive $\delta^{34}S$ or negative $\delta^{34}S$ that implies mixing of sulfide sulfur with different $\delta^{34}S$ before, during, and after the end-Permian mass extinction. The precise coincidence of the negative $\Delta^{33}S$ anomaly with the extinction horizon in western Canada suggests that shoaling of H_2S-rich waters may have driven the end-Permian mass extinction. Our data also imply episodic euxinia and oscillations between sulfidic and oxic conditions during the earliest Triassic, providing evidence of a causal link between incursion of sulfidic waters and the delayed recovery of the marine ecosystem.

end-Permian mass extinction | Panthalassic Ocean | multiple sulfur isotopes | sulfidic waters

The end-Permian mass extinction was the largest biotic catastrophe of the last 540 million years, resulting in the disappearance of >80% of marine species, and a full biotic recovery did not occur until 4–8 million years after the extinction event (1–6). Several lines of evidence from the low paleolatitude Paleotethys and high paleolatitude Boreal oceans, which accounted for ∼10–15% of the contemporaneous global ocean area, suggest that sulfidic (H_2S-rich) conditions may have developed widely during the end-Permian extinction (7–13). However, redox chemistry changes in the Panthalassic Ocean, comprising ∼85–90% of the global ocean area, remain controversial, with competing hypotheses proposing extensive deepwater anoxia ("superanoxic ocean") or suboxic deep waters in combination with spatially constrained thermocline anoxia (14–18). Evidently, redox chemistry changes in the Panthalassic Ocean are central to an examination of the links between global-ocean conditions and the end-Permian extinction event as well as the subsequent delayed biotic recovery.

The preservation of Permian–Triassic boundary deep-sea sediments is limited because most oceanic crust of that age has been subducted, and the only surviving Panthalassic seafloor sediments are within accretionary terranes or marginal uplifts now located in western Canada, Japan, and New Zealand (19, 20). In this study, we report analyses of all four sulfur isotopes (^{32}S, ^{33}S, ^{34}S, and ^{36}S) for pyrite from the deep-sea sediments of western Canada and Japan. Our study samples from western Canada were collected at Opal Creek in southwestern Alberta (50.67542°N, 115.07992°W), which represents an outer shelf or upper slope setting in the eastern Panthalassic Ocean at a paleolatitude of ∼30°N (21, 22) (Fig. 1). A second set of study samples is from Gujo-Hachiman in central Japan (35.7355°N, 136.8489°E), which represents the abyssal plain of the equatorial Panthalassic Ocean (23) (Fig. 1).

The Opal Creek section consists of black shale and siltstone of the lower Phroso Siltstone Member and upper Vega Siltstone Member of the Sulfur Mountain Formation (Fig. 2). The lowermost Sulfur Mountain Formation contains abundant siliceous monaxon sponge spicules and triaxon hyalosponge spicules that disappear abruptly at 0.36 m above the base of the formation (20). The disappearance of sponge spicules coincided with a sudden influx of Late Permian conodonts belonging to the genus *Clarkina*, marking the onset of the end-Permian extinction event (20) (Fig. 2). Four conodont zones were defined at Opal Creek, with the first occurrence of *Hindeodus parvus* and *Clarkina taylorae* indicating the Permian–Triassic boundary (20, 24) (Fig. 2).

The Gujo-Hachiman section consists of three units: Unit I, comprising green–gray ribbon-chert; Unit II, comprising green–gray to black siliceous claystone; and Unit III, comprising black shale with a few thin lenses of gray chert and layers of white–yellow siliceous claystone bearing uppermost Permian radiolarians (17, 18, 25) (Fig. 2). Radiolarian and conodont data suggest that

Significance

To understand how most life on Earth went extinct 250 million years ago, we used multiple sulfur isotopes to investigate redox chemistry changes in the Panthalassic Ocean, comprising ∼85–90% of the contemporaneous global ocean. The S-isotopic anomalies from Canada and Japan provide evidence for the timing of the onset of euxinia and mixing of sulfidic and oxic waters. Our data suggest that shoaling of H_2S-rich waters may have driven the mass extinction and delayed the recovery of the marine ecosystem. This study illustrates how environmental changes could have had a devastating effect on Earth's early biosphere, and may have present-day relevance because global warming and eutrophication are causing development of sulfidic zones on modern continental shelves, threatening indigenous marine life.

Author contributions: Y.S. designed research; T.J.A., C.M.H., and Y.S. collected samples; G.Z., X.Z., D.H., D.L., J.F., L.Q., M.S., D.S., K.C., and Y.S. performed geochemical analysis; G.Z., X.Z., D.H., D.L., T.J.A., J.F., C.M.H., L.Q., S.D.S., K.C., and Y.S. analyzed data; and G.Z. and Y.S. wrote the paper.

The authors declare no conflict of interest.

This article is a PNAS Direct Submission.

Freely available online through the PNAS open access option.

[1]To whom correspondence should be addressed. Email: yashen@ustc.edu.cn.

This article contains supporting information online at www.pnas.org/lookup/suppl/doi:10.1073/pnas.1610931114/-/DCSupplemental.

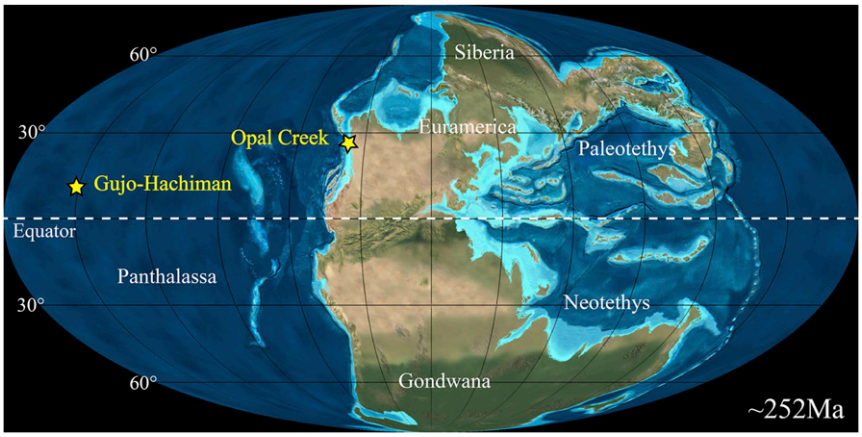

Fig. 1. Paleogeography for the end-Permian world (~252 Ma) and the respective location of the Opal Creek and Gujo-Hachiman sections (18, 22).

the Permian–Triassic boundary is located near the base of Unit III (17, 18, 25, 26).

Exact placement of the end-Permian extinction horizon in the two study sections allows us to use multiple sulfur isotopes to explore temporal changes of redox chemistry in the Panthalassic Ocean and their potential link to the end-Permian mass extinction as well as the following protracted marine biotic recovery.

The multiple sulfur isotope data of pyrite from the Opal Creek and Gujo-Hachiman sections are presented using conventional delta notation: $\delta^{3i}S = 1{,}000 \times (({}^{3i}S/{}^{32}S)_{sample}/({}^{3i}S/{}^{32}S)_{reference} - 1)$, where 3i = 33, 34, or 36. Capital delta notation is also defined to describe relationships involving the least abundant isotopes: $\Delta^{33}S = \delta^{33}S - 1{,}000 \times ((1 + \delta^{34}S/1{,}000)^{0.515} - 1)$, $\Delta^{36}S = \delta^{36}S - 1{,}000 \times ((1 + \delta^{34}S/1{,}000)^{1.90} - 1)$. The capital delta notation is defined with exponents of 0.515 and 1.90 to approximate the deviation from single-step low-temperature equilibrium exchange reactions (27, 28). Delta and capital delta values are given in units of per mille (‰). Figs. 2 and 3 present $\delta^{34}S$ and $\Delta^{33}S$ data of pyrite from the study sections (full analytical data of the samples and reference materials available as Tables S1–S3).

Before the end-Permian extinction, $\delta^{34}S$ compositions at Opal Creek vary from –24.97‰ to –10.17‰ with $\Delta^{33}S$ from –0.028‰ to +0.021‰ (Fig. 2). In the same interval at Gujo-Hachiman, $\delta^{34}S$ ranges from –40.18‰ to +13.27‰ with $\Delta^{33}S$ from –0.099‰ to +0.095‰ (Fig. 2). The end-Permian extinction horizon at Opal Creek (sample Chang+28) exhibits $\delta^{34}S$ of –23.06‰ and $\Delta^{33}S$ of –0.017‰ (Fig. 2). The same horizon at Gujo-Hachiman (sample

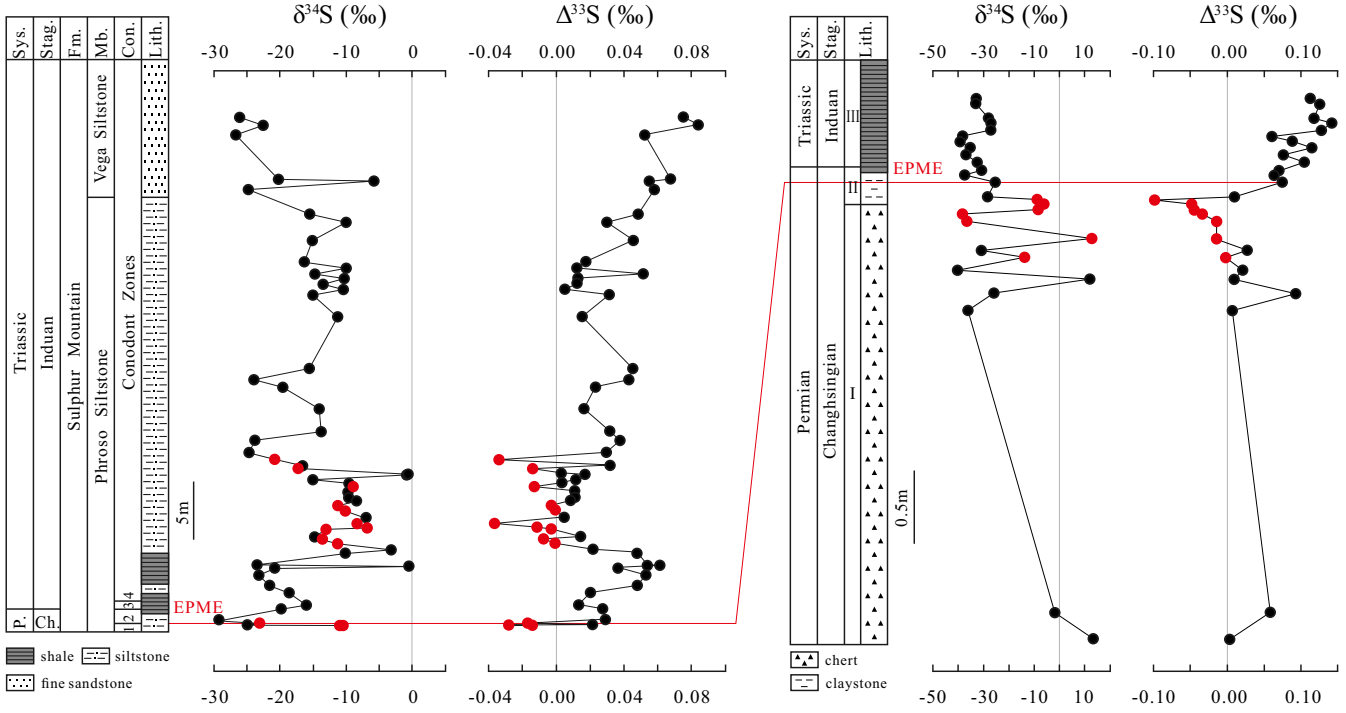

Fig. 2. Permian-Triassic biostratigraphy and multiple S-isotopic data for the Opal Creek (*Left*) and Gujo-Hachiman (*Right*) sections (filled red circles indicate negative $\Delta^{33}S$). The red line corresponds to the end-Permian mass extinction horizon (EPME). Conodont Zonation at Opal Creek is after refs. 20 and 24: (1) *Mesogondolella sheni* Zone; (2) *Clarkina hauschkei–Clarkina meishanensis* Zone; (3) *H. parvus–C. taylorae* Zone; (4) *C. taylorae–Clarkina cf. carinata* Zone.

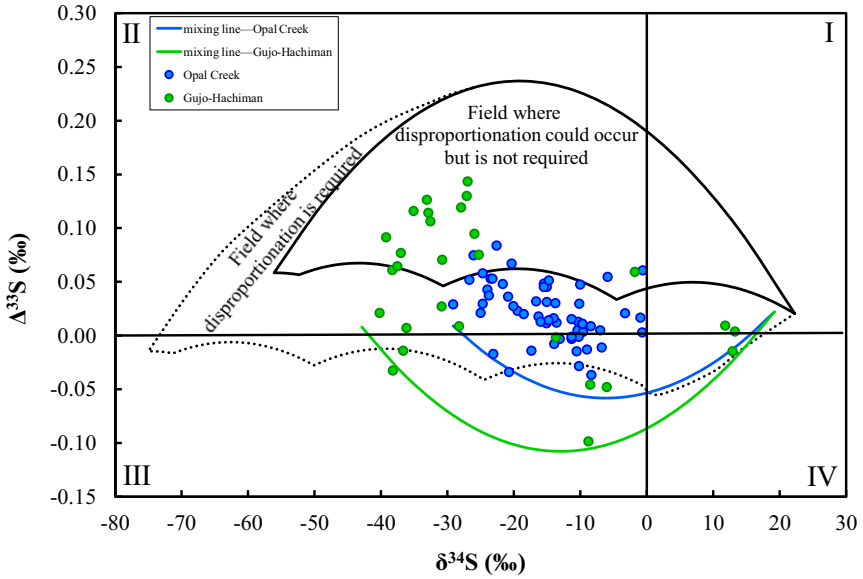

Fig. 3. Cross-plot of $\delta^{34}S$ vs. $\Delta^{33}S$ for pyrite from the Opal Creek and Gujo-Hachiman sections. The colored nonlinear line represents a mixing line generated by the model (blue: Opal Creek, green: Gujo-Hachiman). The model field for sulfate reduction (black outlined field) and sulfate reduction combined with disproportionation (black dotted-line field) represent the field of all possible fractionations predicted by a model of sulfate reducers, and is larger than in ref. 12 because that field was calculated for a more limited range of fractionations produced by experiments with sulfate reducers. Whereas the expanded range of the model field may capture solutions that are non–steady-state, it provides a more conservative set of criteria to identify a mixing scenario than the field plotted by ref. 12.

ITJ-13) displays $\delta^{34}S$ of –25.24‰ and $\Delta^{33}S$ of +0.075‰ (Fig. 2). After the end-Permian extinction, $\delta^{34}S$ at Opal Creek varies from –29.14‰ to –0.59‰ with $\Delta^{33}S$ from –0.037‰ to +0.084‰ (Fig. 2). For the same interval, the Gujo-Hachiman section shows $\delta^{34}S$ values from –39.21‰ to –26.95‰ with $\Delta^{33}S$ of +0.061‰ to +0.143‰ (Fig. 2).

We use a previously described box model (29–32) to evaluate the significance of variation in our multiple sulfur isotopes for redox chemistry changes in the Panthalassic Ocean. In this model, covariation of $\delta^{34}S$ and $\Delta^{33}S$ and their positions in Quadrants I–IV provide insight regarding the sulfate reduction, sulfur oxidation, and sulfur disproportionation processes (Fig. 3) (calculations available in *Sulfur-Cycle Model*; Figs. S1 and S2). The model adopts an isotopic composition for seawater of $\delta^{34}S$ = +19.2‰ and $\Delta^{33}S$ = +0.022‰, as estimated from multiple S-isotopic analysis of contemporaneous marine carbonate-associated sulfate (33).

At Opal Creek before the end-Permian mass extinction, pyrite shows negative $\delta^{34}S$ in combination with either positive $\Delta^{33}S$ (Quadrant II) or negative $\Delta^{33}S$ (Quadrant III) (Figs. 2 and 3). At the extinction horizon, pyrite exhibits negative $\Delta^{33}S$ with negative $\delta^{34}S$ (Quadrant III) (Figs. 2 and 3). After the extinction, pyrite shows positive $\Delta^{33}S$ with negative $\delta^{34}S$ (Quadrant II) (Figs. 2 and 3). However, negative $\Delta^{33}S$ with negative $\delta^{34}S$ values (Quadrant III) are observed for an interval between ∼7 m and ∼14 m (Figs. 2 and 3). Higher in the Sulfur Mountain Formation, all multiple S-isotopic data show positive $\Delta^{33}S$ with negative $\delta^{34}S$ (Quadrant II) (Figs. 2 and 3).

At Gujo-Hachiman before the extinction event, the lower to middle part of Unit I exhibits positive $\Delta^{33}S$ with positive $\delta^{34}S$ (Quadrant I) or negative $\delta^{34}S$ (Quadrant II) (Figs. 2 and 3). The upper part of Unit I and lower Unit II are characterized by negative $\Delta^{33}S$ (Quadrants III and IV) except for two samples with positive $\Delta^{33}S$ (Quadrant II) (Figs. 2 and 3). The extinction horizon exhibits positive $\Delta^{33}S$ with negative $\delta^{34}S$ (Quadrant II), as do all samples from higher in the section (Figs. 2 and 3).

The paleoenvironmental significance of multiple S-isotopic data from the Opal Creek and Gujo-Hachiman sections can be inferred based on their positions in Quadrants I–IV (Fig. 3). Data in Quadrant II (positive $\Delta^{33}S$ with negative $\delta^{34}S$) may be due to fractionation relationships produced by microbial sulfate reduction, disproportionation of sulfur intermediate compounds, and the conservation of mass in the sulfur cycle (30). Quadrant II samples situated within the sulfate reduction field (black outlined field) imply sulfate reduction in an open system in which disproportionation could occur, but is not required (Fig. 3). However, other samples in Quadrant II (positive $\Delta^{33}S$ with negative $\delta^{34}S$) as well as two samples in Quadrant I (positive $\Delta^{33}S$ with positive $\delta^{34}S$) are situated outside the sulfate reduction field but within the sulfur disproportionation field (black dotted-line field), suggesting that they may have been produced by a combination of sulfate reduction and sulfur disproportionation (Fig. 3). It is important to note that the inclusion of sulfur disproportionation in our model is not to imply that this process must occur in any of these environments, but simply because its operation will expand the field of steady-state solutions and reduce the possibility of false identification of mixing scenarios.

S-isotopic data in Quadrants III and IV cannot be attributed simply to either sulfate reduction and/or sulfur disproportionation (12, 29, 34). Although a few negative $\Delta^{33}S$ values within the disproportionation field might be due to a combination of sulfate reduction and sulfur disproportionation (Fig. 3), this interpretation is not strongly supported by observations from biological experiments of sulfate reduction and/or sulfur disproportionation. Biological culture experiments have shown that, under sulfate-unlimited conditions, sulfide produced by sulfate reduction is more enriched in ^{33}S compared with reactant sulfate (35–37). Under sulfate-limited conditions, the sulfide generated by sulfate reduction should have similar $\delta^{34}S$ and $\Delta^{33}S$ to the reactant sulfate if the latter is completely reduced. Also, culture experiments of sulfur disproportionation have shown that products of sulfide and sulfate are enriched in ^{33}S relative to the reactant elemental sulfur (38). In this case, the negative $\Delta^{33}S$ projected by the model may be due to the specified boundary conditions used in the model, e.g., the proportion between sulfide that is reoxidized and disproportionated and sulfide produced by sulfate reduction. Previous

studies have shown that mixing of sulfide having strongly negative $\delta^{34}S$ and positive $\Delta^{33}S$ with sulfide having positive $\delta^{34}S$ and positive $\Delta^{33}S$ (the latter being similar to seawater sulfate) can produce sulfide with negative $\Delta^{33}S$ values (12, 29, 34). This negative $\Delta^{33}S$ mixing signature is thus interpreted to account for the negative $\Delta^{33}S$ compositions observed in the Opal Creek and Gujo-Hachiman sections.

Negative $\Delta^{33}S$ compositions have been linked to shoaling of sulfidic waters and resultant mixing of sulfidic and oxic waters in the Permian oceans before or coincident with the mass extinction (12, 29). In this interpretation, shoaling of sulfidic waters changed the sulfur cycle within the sediment, yielding a mixture of pyrite already formed in an open-system environment with pyrite formed in a nearly closed-system environment caused by a sharp reduction of bioturbation as a result of the demise of benthic fauna by sulfide poisoning.

Two endmembers were used to generate the mixing lines in Fig. 3. One endmember is the isotopic composition of latest Permian–Early Triassic seawater sulfate and the other is the most negative $\delta^{34}S$ value observed at Opal Creek and Gujo-Hachiman, respectively (Fig. 3). The ranges of the mixing lines encompass all negative $\Delta^{33}S$ data from the two study sections (Fig. 3).

Before the end-Permian extinction, a combination of negative $\delta^{34}S$ and $\Delta^{33}S$ values indicates shoaling of sulfidic waters and transition to and from sulfidic condition at Opal Creek (Fig. 2). A similar pattern in the correlative interval at Gujo-Hachiman also provides evidence for the timing of the onset of euxinia and oscillations between sulfidic and oxic conditions (Fig. 2). These results are consistent with the multiple S-isotopic data from the Paleotethys Ocean that suggest shoaling of sulfidic waters and resultant mixing of sulfidic and oxic waters before the end-Permian mass extinction event (12) (Fig. 4). Our multiple S-isotopic data from Opal Creek and Gujo-Hachiman thus imply that shoaling of sulfidic waters and oscillations between sulfidic and oxic conditions may be of global significance before the end-Permian extinction.

The negative $\Delta^{33}S$ with negative $\delta^{34}S$ at Opal Creek coincided exactly with the extinction horizon, linking sulfidic conditions to the extinction event (Figs. 2 and 4). This observation suggests that shoaling of sulfidic waters and oscillations between sulfidic and oxic conditions may have driven the end-Permian mass extinction. The lack of negative $\Delta^{33}S$ during the extinction at Gujo-Hachiman (Figs. 2 and 4) might reflect preservation biases, which could be tested by future multiple S-isotopic analyses of pyrite from the extinction horizon in other sections.

Above the end-Permian mass extinction horizon, positive $\Delta^{33}S$ with negative $\delta^{34}S$ values are present in the Opal Creek and Gujo-Hachiman sections (Fig. 2). At Opal Creek, abundant small framboidal pyrites and trace metal data provide evidence that the lower 4 m of the Sulfur Mountain Formation were deposited under sulfidic conditions (22). The absence of negative $\Delta^{33}S$ values in this interval and Unit III at Gujo-Hachiman suggests that accumulation of abundant syngenetic pyrite having positive $\Delta^{33}S$ compositions overwhelmed the signal of negative $\Delta^{33}S$, consistent with sustained euxinic conditions. The reappearance of negative $\Delta^{33}S$ above this interval at Opal Creek (Figs. 2 and 4) provides evidence of an episodic incursion of sulfidic waters and oscillations between sulfidic and oxic conditions during the Early Triassic. Conditions of this type may have contributed to the delayed marine biotic recovery, as reflected in the disappearance of benthic fauna and bioturbation in the Phroso Siltstone Member of the Sulfur Mountain Formation (20).

Our multiple S-isotopic study provides insights into temporal changes of redox chemistry in the latest Permian–Early Triassic Panthalassic Ocean. Our data suggest that episodic shoaling of sulfidic waters, oscillations between sulfidic and oxic conditions, and related environmental deterioration led up to the end-Permian extinction. The negative $\Delta^{33}S$ anomaly at the extinction horizon at Opal Creek provides critical evidence that shoaling of sulfidic waters and oscillations between sulfidic and oxic conditions may have been the main killing agents during the mass extinction. Moreover, the episodic incursion of sulfidic waters and mixing of

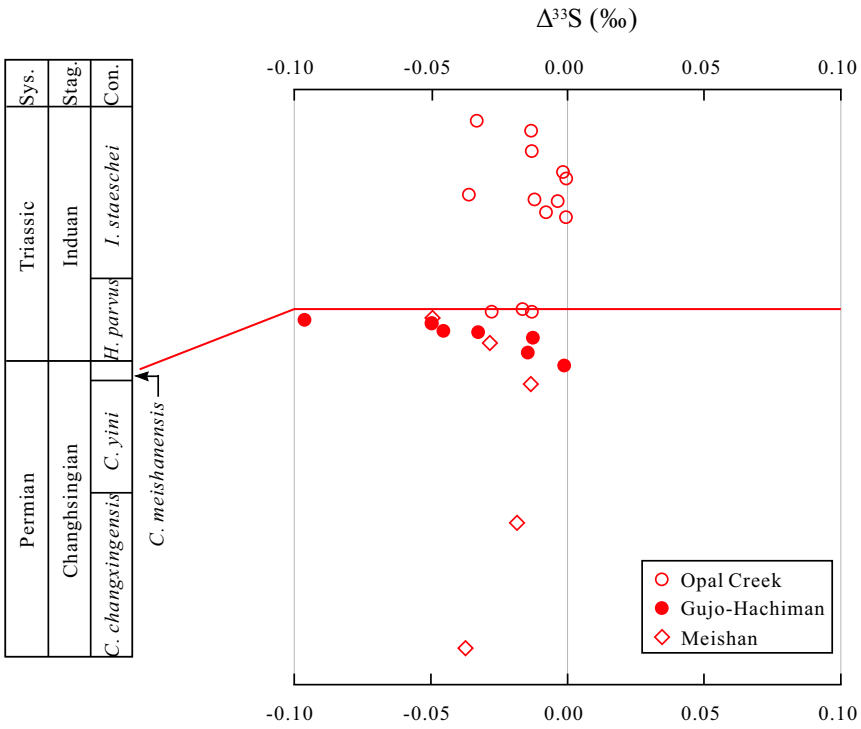

Fig. 4. The negative $\Delta^{33}S$ data from Opal Creek and Gujo-Hachiman (this study) and from Meishan (12) are aligned using the extinction horizon as a datum. The thickness of each conodont zone is not to scale.

sulfidic and oxic waters indicated by our multiple S-isotopic data may have played an important role in the protracted marine biotic recovery from the end-Permian mass extinction. Future isotopic studies carried out in the framework of biostratigraphy and sedimentary facies worldwide can test our model and improve our understanding of the relationships between redox chemistry changes and the mass extinction as well as biotic recovery.

Methods

Pyrite sulfur was extracted and trapped as Ag_2S (39). During this procedure, the product H_2S was carried by nitrogen gas through a condenser and a bubbler filled with milli-Q water, and collected as silver sulfide by reacting with silver nitrate solution.

For multiple S-isotopic analysis, Ag_2S was converted to SF_6 quantitatively by a fluorination reaction in a Ni reaction vessel with a 10-fold excess of F_2 at 250 °C for 8 h (12). After the reaction, SF_6 was purified cryogenically by distillation in a liquid N_2–ethanol slurry at −110 °C, and chromatographically on a 120 molecular sieve 5 Å/Hasep Q column with a thermal conductivity detector (TCD). The He carrier flow was set at 20 mL/min. The SF_6 peak was registered on a TCD and then isolated by freezing into a liquid-nitrogen-cooled trap. The isotopic abundance of the purified SF_6 was analyzed on a Finnigan MAT 253 at m/e^- values of 127, 128, 129, and 131 ($^{32}SF_5^+$, $^{33}SF_5^+$, $^{34}SF_5^+$, $^{36}SF_5^+$).

One-sigma uncertainties on mass-dependent reference materials are better than ±0.2‰, ±0.01‰, and ±0.2‰ in $\delta^{34}S$, $\Delta^{33}S$, and $\Delta^{36}S$, respectively. Uncertainties on the measurements reported here are estimated to be better than ±0.2‰, ±0.01‰, and ±0.2‰ for $\delta^{34}S$, $\Delta^{33}S$, and $\Delta^{36}S$, respectively.

ACKNOWLEDGMENTS. We thank three anonymous reviewers for comments. This study was supported by National Natural Science Foundation of China (41330102 and 41520104007), and the 111 Project (Y.S.) and the Fundamental Research Funds for the Central Universities (L.Q.). T.J.A. and J.F. were supported by the National Science Foundation and C.M.H. was supported by Natural Sciences and Engineering Research Council of Canada.

1. Erwin DH (2006) *Extinction: How Life on Earth Nearly Ended 250 Million Years Ago* (Princeton University Press, Princeton).
2. Stanley SM (2016) Estimates of the magnitudes of major marine mass extinctions in earth history. *Proc Natl Acad Sci USA* 113(42):E6325–E6334.
3. Knoll AH, Bambach RK, Payne JL, Pruss S, Fischer WW (2007) Paleophysiology and end-Permian mass extinction. *Earth Planet Sci Lett* 256(3-4):295–313.
4. Payne JL, et al. (2004) Large perturbations of the carbon cycle during recovery from the end-permian extinction. *Science* 305(5683):506–509.
5. Shen SZ, et al. (2011) Calibrating the end-Permian mass extinction. *Science* 334(6061): 1367–1372.
6. Chen Z-Q, Benton MJ (2012) The timing and pattern of biotic recovery following the end-Permian mass extinction. *Nat Geosci* 5(6):375–383.
7. Nielsen JK, Shen Y (2004) Evidence for sulfidic deep water during the Late Permian in the East Greenland Basin. *Geology* 32(12):1037–1040.
8. Grice K, et al. (2005) Photic zone euxinia during the Permian-triassic superanoxic event. *Science* 307(5710):706–709.
9. Riccardi AL, Arthur MA, Kump LR (2006) Sulfur isotopic evidence for chemocline upward excursions during the end-Permian mass extinction. *Geochim Cosmochim Acta* 70(23):5740–5752.
10. Cao C, et al. (2009) Biogeochemical evidence for euxinic oceans and ecological disturbance presaging the end-Permian mass extinction event. *Earth Planet Sci Lett* 281(3-4):188–201.
11. Algeo TJ, et al. (2008) Association of ^{34}S-depleted pyrite layers with negative carbonate $\delta^{13}C$ excursions at the Permian-Triassic boundary: Evidence for upwelling of sulfidic deep-ocean water masses. *Geochem Geophys Geosyst* 9:Q04025, 10.1029/2007GC001823.
12. Shen Y, et al. (2011) Multiple S-isotopic evidence for episodic shoaling of anoxic water during Late Permian mass extinction. *Nat Commun* 2:210, 10.1038/ncomms1217.
13. Schobben M, et al. (2015) Flourishing ocean drives the end-Permian marine mass extinction. *Proc Natl Acad Sci USA* 112(33):10298–10303.
14. Isozaki Y (1997a) Permo-Triassic boundary superanoxia and stratified superocean: Records from lost deep sea. *Science* 276(5310):235–238.
15. Kato Y, Nakao K, Isozaki Y (2002) Geochemistry of Late Permian to Early Triassic pelagic cherts from southwest Japan: Implications for an oceanic redox change. *Chem Geol* 182(1):15–34.
16. Kakuwa Y (2008) Evaluation of palaeo-oxygenation of the ocean bottom across the Permian-Triassic boundary. *Global Planet Change* 63(1):40–56.
17. Algeo TJ, et al. (2010) Changes in productivity and redox conditions in the Panthalassic Ocean during the latest Permian. *Geology* 38(2):187–190.
18. Algeo TJ, et al. (2011) Spatial variation in sediment fluxes, redox conditions, and productivity in the Permian-Triassic Panthalassic Ocean. *Palaeogeogr Palaeoclimatol Palaeoecol* 308(1-2):65–83.
19. Isozaki Y (1997b) Jurassic accretion tectonics of Japan. *Isl Arc* 6(1):25–51.
20. Henderson CM (1997) Uppermost Permian conodonts and the Permian-Triassic boundary in the Western Canada sedimentary basin. *Bull Can Pet Geol* 45(4):693–707.
21. Henderson CM (1989) Absaroka sequence. The lower Absaroka sequence: Upper Carboniferous and Permian. *Western Canada Sedimentary Basin: A Case History*, ed Ricketts B (Canadian Society of Petroleum Geologists, Calgary, AB, Canada), pp 203–217.
22. Schoepfer SD, et al. (2013) Termination of a continent-margin upwelling system at the Permian-Triassic boundary (Opal Creek, Alberta, Canada). *Global Planet Change* 105:21–35.
23. Ando A, Kodama K, Kojima S (2001) Low-latitude and Southern Hemisphere origin of Anisian (Triassic) bedded chert in the Inuyama area, Mino terrane, central Japan. *J Geophys Res* 106(B2):1973–1986.
24. Schoepfer SD, Henderson CM, Garrison GH, Ward PD (2012) Cessation of a productive coastal upwelling system in the Panthalassic Ocean at the Permian–Triassic boundary. *Palaeogeogr Palaeoclimatol Palaeoecol* 313-314:181–188.
25. Kuwahara K, Yao A (2001) Late Permian radiolarian faunal change in bedded chert of the Mino Belt, Japan. *News Osaka Micropaleontol* 12:33–49.
26. Yao J, Yao A, Kuwahara K (2001) Upper Permian biostratigraphic correlation between conodont and radiolarian zones in the Tamba-Mino Terrane, southwest Japan. *J Geosci Osaka City Univ* 44:97–119.
27. Hulston JR, Thode HG (1965) Variations in the S^{33}, S^{34}, and S^{36} contents of meteorites and their relation to chemical and nuclear effects. *J Geophys Res* 70(14):3475–3484.
28. Farquhar J, Wing BA (2003) Multiple sulfur isotopes and the evolution of the atmosphere. *Earth Planet Sci Lett* 213(1-2):1–13.
29. Zhang GJ, et al. (2015) Widespread shoaling of sulfidic waters linked to the end-Guadalupian (Permian) mass extinction. *Geology* 43(12):1091–1094.
30. Farquhar J, Johnston DT, Wing BA (2007) Implications of conservation of mass effects on mass-dependent isotope fractionations: Influence of network structure on sulfur isotope phase space of dissimilatory sulfate reduction. *Geochim Cosmochim Acta* 71(24):5862–5875.
31. Johnston DT, et al. (2005) Active microbial sulfur disproportionation in the Mesoproterozoic. *Science* 310(5753):1477–1479.
32. Brunner B, Bernasconi SM (2005) A revised isotope fractionation model for dissimilatory sulfate reduction in sulfate reducing bacteria. *Geochim Cosmochim Acta* 69(20):4759–4771.
33. Wu NP, Farquhar J, Strauss H, Kim S-T, Canfield DE (2010) Evaluating the S-isotope fractionation associated with Phanerozoic pyrite burial. *Geochim Cosmochim Acta* 74(7):2053–2071.
34. Sim MS, Ono S, Hurtgen MT (2015) Sulfur isotope evidence for low and fluctuating sulfate levels in the Late Devonian ocean and the potential link with the mass extinction event. *Earth Planet Sci Lett* 419:52–62.
35. Johnston DT, Farquhar J, Canfield DE (2007) Sulfur isotope insights into microbial sulfate reduction: When microbes meet models. *Geochim Cosmochim Acta* 71(16): 3929–3947.
36. Sim MS, Ono S, Donovan K, Templer SP, Bosak T (2011a) Effect of electron donors on the fractionation of sulfur isotopes by a marine *Desulfovibrio* sp. *Geochim Cosmochim Acta* 75(15):4244–4259.
37. Sim MS, Bosak T, Ono S (2011b) Large sulfur isotope fractionation does not require disproportionation. *Science* 333(6038):74–77.
38. Johnston DT, et al. (2005) Multiple sulfur isotope fractionations in biological systems: A case study with sulfate reducers and sulfur disproportionators. *Am J Sci* 305(6-8): 645–660.
39. Canfield DE, Raiswell R, Westrich JT, Reaves CM, Berner RA (1986) The use of chromium reduction in the analysis of reduced inorganic sulfur in sediments and shales. *Chem Geol* 54(1-2):149–155.